

EXPERIMENTAL INVESTIGATION OF MULTILAYER SURFACING SYSTEM ON ORTHOTROPIC STEEL BRIDGE WITH THE FIVE-POINT BENDING TEST

George Tzimiris¹, Xueyan Liu², Tom Scarpas³, Jinlong⁴, Rob Hofman⁵, Jan Voskuilen⁶

⁽¹⁾ Corresponding author

Section of Structural Mechanics, Delft University of Technology

Stevinweg 1, 2628 CN Delft, the Netherlands

Phone: + 31 (0)15 27 89388

Email: g.tzimiris@tudelft.nl

⁽²⁾ Section of Structural Mechanics, Delft University of Technology

Stevinweg 1, 2628 CN Delft, the Netherlands

Phone: + 31 (0)15 27 87918

Email: x.liu@tudelft.nl

⁽³⁾ Section of Structural Mechanics, Delft University of Technology

Stevinweg 1, 2628 CN Delft, the Netherlands

Phone: + 31 (0)15 27 84017

Email: a.scarpas@tudelft.nl

⁽⁴⁾ Section of Structural Mechanics, Delft University of Technology

Stevinweg 1, 2628 CN Delft, the Netherlands

Phone: + 31 (0)15 27 84676

Email: jinlong.li@tudelft.nl

⁽⁵⁾ Rijkswaterstaat, Centre for Traffic and Navigation

Schoenmakerstraat, 2628 VK Delft, the Netherlands

Phone: + 31 (0)887982284

Email: rob.hofman@rws.nl

⁽⁶⁾ Rijkswaterstaat, Centre for Traffic and Navigation

Schoenmakerstraat, 2628 VK Delft, the Netherlands

Phone: + 31 (0)88 79823042

Email: jan.voskuilen@rws.nl

Submission Date: 01/08/2012

Word Count:

Body Text = 3000

Figures 14×250 = 3500

Tables 4×250 = 1000

Total = 7500

ABSTRACT

Due to lightweight and flexibility, orthotropic steel deck bridges become popular the last decades but several problems were reported in relation to asphalt surfacing materials such as rutting, cracking, loss of bond between the surfacing system and steel deck. In the Netherlands a surfacing structure for orthotropic steel bridge decks mostly consists of five structural layers: top porous asphalt layer, guss asphalt layer, steel deck and two membrane layers.

The five-point bending fatigue test is the standard device in France for asphalt concrete used on steel orthotropic deck bridges to perform the best asphalt mixture having a strong resistance to cracking. For the needs of this paper the 5 PBT was employed in order to evaluate the performance of the whole multilayer structure on steel deck and also to evaluate the mechanical properties of both top and bottom membrane and the influence they have on the structure.

For the completion of the experimental investigation two types of specimen have been tested using the 5PBT set up. Displacement sensors have been used in order to detect the initiation of cracks where they are most likely to appear. Strain gauges have been used in order to monitor significant changes in strain on the Guss asphalt layer during the fatigue tests. Shear displacements between the asphalt layers are monitored and presented. It shows that the stiffness and the bonding characteristics of the intermediate membrane sheet as well as the wearing course behaviour seem to have great influence on the mechanical response of multilayer bridge surfacing system.

Keywords: Five-point bending test; orthotropic steel deck bridge; multilayer surfacing system;

1 INTRODUCTION

2 Orthotropic steel bridges consist of a 10-14 mm steel deck plate supported in two perpendicular
 3 directions, by U-shaped stiffeners and crossbeams in the longitudinal and transverse direction
 4 respectively[1]. Due to lightweight and flexibility orthotropic steel decks have, become popular in the
 5 last decades but several problems were reported in relation to asphalt surfacing materials such as
 6 rutting, cracking, loss of bond between the surfacing system and steel deck [2].

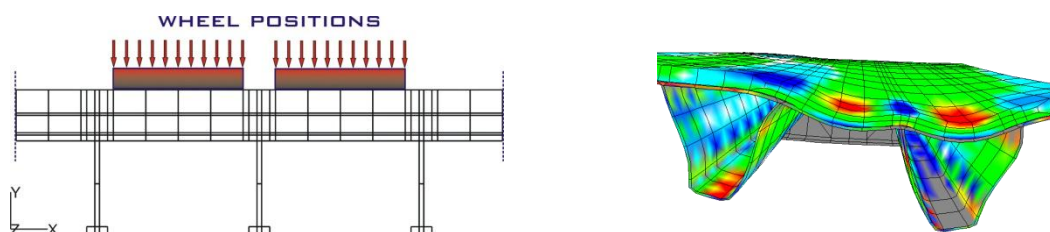
7 The five point bending test (5PBT) is a laboratory scale test that allows studying the fatigue
 8 resistance of surfacing layers on orthotropic bridge decks [3]. Hameau et al. (1981) reported the most
 9 severe load case for surfacing layers of orthotropic bridge decks is when they are subjected to
 10 negative moments.. The 5PBT has become a French standard test method (NF-P98-286, 2006) [4].

11 For the purposes of this paper, the 5PBT was performed in order to understand if this type of
 12 test can be directly used to evaluate the performance of the multilayer system on steel deck and also to
 13 perform a laboratory scale test that would allow studying the fatigue resistance of surfacing layers on
 14 orthotropic bridge decks.

15 In the first part of this paper the experimental device of the 5PBT, test conditions and
 16 instrumentation are described. In the second part of this paper, results of 5PBT specimens with two
 17 different membrane products as bonding layers at two temperatures -5°C and $+10^{\circ}\text{C}$ are exposed.
 18 This paper shows that the in time deformation measurements are allowable to evaluate the fatigue
 19 response of the wearing course. The stiffness and the bonding characteristics of the intermediate
 20 membrane sheet as well as the wearing course behaviour seem to have great influence on the
 21 mechanical response of multilayer bridge surfacing system.

22 DESCRIPTION OF THE FIVE-POINT BENDING TEST

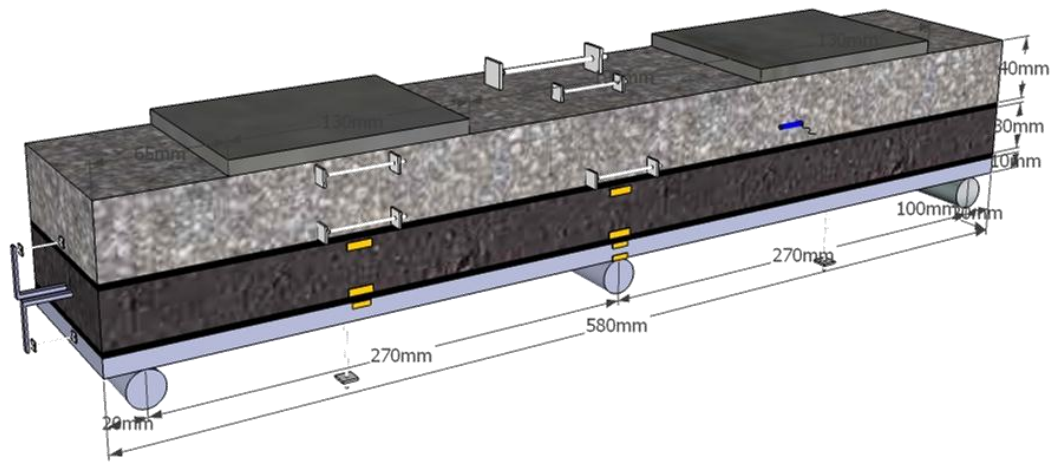
23 In order to assess the fatigue resistance of the steel bridge multi-layer surfacing system The French
 24 five-point bending test (5PBT) has been used. It was developed by the ‘‘Laboratoire Central des Ponts
 25 et Chaussées’’(LCPC) in the 70s, and its main advantage is the ability to safely represent the
 26 conditions on a real steel deck applying negative moments [4]. This occur at the alignment of the
 27 stiffener web when each of the wheel of a double tyre is positioned at each side of the web Figure 1



28
29 **FIGURE 1 Schematic representation of the area of concern**

30 In the Netherlands an asphaltic surfacing structure for orthotropic steel deck bridge mostly consists of
 31 two structural layers, Figure 2. The upper layer consists of Porous Asphalt (PA) because of reasons
 32 related to noise hindrance. For the lower layer a choice between Mastic Asphalt (MA) or Guss
 33 Asphalt (GA), can be made [5]. Therefore, in order to study the fatigue response of the typical Dutch
 34 steel deck bridge, 5PBT specimen with the two wearing course bonded by two membrane sheets are
 35 investigated.

36 The specimen is consisted of 10 mm-thick steel plate, 2 to 4mm-thick bottom membrane,
 37 30mm Guss asphalt layer, 4.7-4.8mm-thick top membrane and 40mm thickness of porous asphalt
 38 layer, see Figure 2.



39

40

FIGURE 2 Specimen geometry and composition

41 For the specimen preparation a steel plate with 580 mm x 100mm x 10mm was used. Two
 42 different types of sample have been prepared by using membrane products A1 and A2 from company
 43 A and B1, B2 from Company B as bonding layer.

44 *Tested materials*

45 **Membrane A1 and A2 from Company A**

46 Product A1 (bottom membrane) is a single ply membrane with a total thickness of 2.4 mm, with non-
 47 woven polyester fleece. This product is made for the single-ply sealing under stone mastic asphalt,
 48 mastic asphalt or bituminous concrete.

49 Product A2 (top membrane) is a single ply membrane with a total thickness of 4.7 mm, which
 50 contains a 1.5 mm strong fleece. This membrane is provided with a modified bituminous mass of 1.6
 51 mm thickness on both sides. It is easy to lay as waterproofing membrane for bridges, and high
 52 resistance to traffic loading. The details of specifications for product A1 and A2 are shown in Table 1.

53

Table 1 Specifications of product A1 and A2 from Company A[10]

Test and specification	Units	Standard	A1	A2
Thickness	mm	EN 1859-2	2.4	4.7
Dimensions	m	EN 1849-2	1.00-7.5	1.00-7.5
Water tightness	6bar /24h	EN 1928-B	o.k.	0.k.
Cold bend test	°C	EN 495-5	-40	-40
Tensile strength at break (20°C,100mm/min)	N/50 mm	EN 12311-1	1445	1115
Elongation at break (20°C, 100mm/min)	%	EN 12311-1	50	35
Debonding Force at (-5C/10C) on steel/membrane interface	N		3410/3100	
Debonding Force at (-5C/10C) on membrane/Guss interface	N		2210/2230	
Debonding Force at (-5C/10C) on membrane/Guss interface	N			2400/2420
Debonding Force at (-5C/10C) on membrane/Porous interface	N			2140/2500

54 **Product B1 and B2 from Company B**

55 Product B1 and B2 are highly performed waterproofing membrane manufactured with SBS
 56 elastomeric bitumen and internally reinforced with a non-woven polyester textile. These two products
 57 are implemented on concrete deck, steel deck, sand asphalt or asphalt concrete.

58 Product B1 and B2 can be bonded to the prepared substrate by melting the film on the
 59 membrane surface and softening of the bitumen. Details of the product specifications can be seen in
 60 Table 2.

61 The mix composition of porous asphalt concrete and Guss asphalt is shown in Table 3.

62 **Table 2 Specifications of product B1 and B2 from Company B[10]**

Test and specification	Units	Standard	B1		B2	
			Nominal values	Critical values	Nominal values	Critical values
Main surface thickness	mm	EN 1849-1	4	3.8	4.8	4.6
Longitudinal overlap width	mm	EN 1848-3			110	100
Tensile strength at break (20°C,100mm/min)	N/5cm	EN 12311-1	950	820	950	820
Elongation at break (20°C, 100mm/min)	%	EN 12311-1	40	35	40	35
Pull-off resistance (20°C, 1.65 m/min)	MPa	NF P 98 282			>0.4	
Cold temperature flexibility	°C	EN 1109	-15	-10	-15	-10
Dimensional stability	%	EN 1107-1			≤0.5	
Heat flow	°C	EN 1110			100	95
Weight/sqm	kg		5.05	4.79	6.27	
Length × width	m×m		10×1	9.9×0.99	8(±10)	1(±0.1)
Weight/roll	kg		50.5	48	48.9	
Debonding Force at (-5C/10C) on steel/membrane interface	N		1040/1104			
Debonding Force at (-5C/10C) on membrane/Guss interface	N		1433/1280			
Debonding Force at (-5C/10C) on membrane/Guss interface	N				1770/1564	
Debonding Force at (-5C/10C) on membrane/Porous interface	N				1940/1520	

64

Table 3 specification for the asphalt mixtures

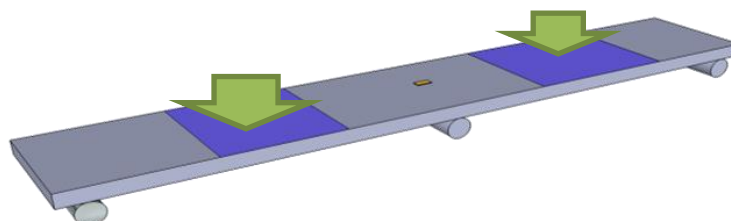
Guss asphalt	Mass percentages (%)		
	Targeted	Min	Max
C8	2.1		
2mm	52	1.1	3.1
63µm	78	45	59
Bitumen MA 8 SFB-5-20(JR)	9.0 (%)	76	80
Porous asphalt			
C11.2		0	8.4
C8		51.0	63.0
C 5.6		71.0	83.0
2mm		81.0	89.0
63µm		94.0	97
Bitumen 50/50	4.9(%)		

65

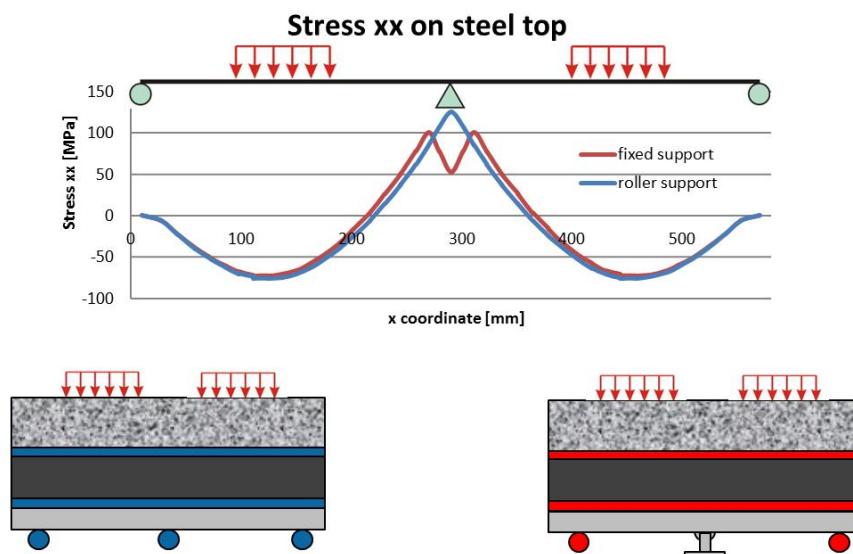
66 *Calibration of the set up*

67 The French standard NF P 98-286 recommends the testing procedures to begin with a calibration
68 phase in order to determine the load corresponding to a strain of $625\mu\text{m}/\text{m}$ on the steel plate surface
69 over the central support[6]. However due to immense differences on the test set up (specimen
70 geometry, specimen composition, steel plate thickness, free central support) the calibration process
71 changed taking into account direct the maximum dual wheel load which corresponds to load pressure
72 of 0.707MPa , see Figure 3. This load pressure corresponds with 9.2 kN on each shoe ($0.707\text{MPa} \times$
73 $130\text{mm} \times 100\text{mm}$), which means a total of 18.4kN . If the same pressure load of 0.707MPa is applied
74 on a wheel print type B (double tyre 220mm by 320mm), it corresponds with 100kN wheel load
75 which is typical truck load utilized in the Netherland.

76

77 **FIGURE 3 Schematic show of a dual wheel load on orthotropic steel bridge and 5PBT**78 *Boundary effect*

79 The fixed central support has replaced with roller support for this set up however higher stress
80 concentration can be observed at the central support at the top face of the steel as it can be seen in
81 finite element simulation in Figure 4. That proves the current set up at same loading condition
82 becomes more flexible than the one with fixed central support condition.



83

84

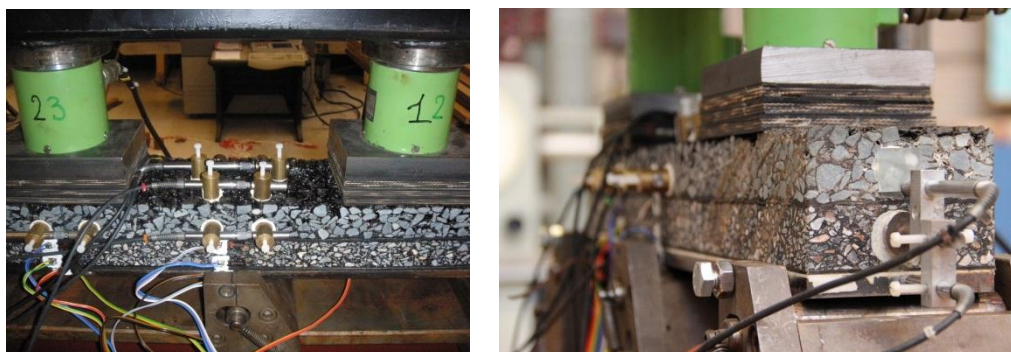
FIGURE 4 Stress concentration at central support

85

Instrumentation

86 Nine strain gauges has been glued on each sample. Two different displacement sensors of the LVDT
 87 (Linear Variable Differential Transformer) [7] type are positioned on the upper face of the sample at
 88 the center, see Figure 5 . Both accuracy and a large detection area are ensured: the first sensor (LVDT
 89 1: ± 2.5 mm and $l=60$ mm) is certain to have a measurement zone where cracks are likely to appear,
 90 and the second (LVDT 2: ± 1.0 mm) and $l=30$ mm) senses the displacements more precisely.

91



92

93

94

FIGURE 5 Instrumentation of Strain gauges and LVTDs on the specimen

95

96

Experimental set up

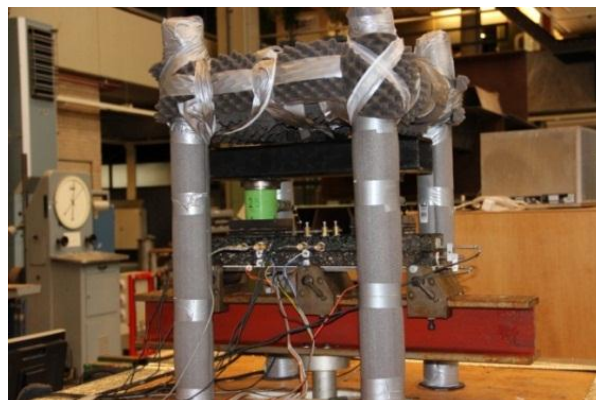
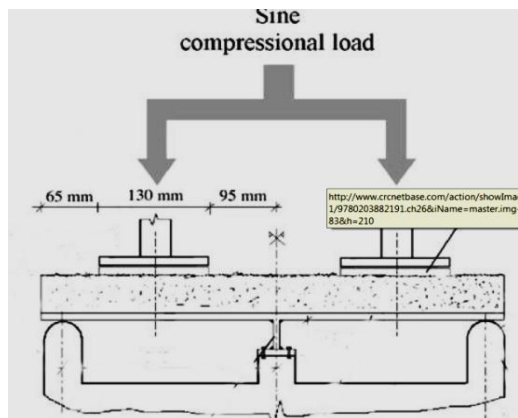
97 In order to run the tests under temperature control the set up needed to properly insulated, Figure 6.

98 A climate chamber was fitted to the 5PBT set up to enable testing under different temperatures.

99 For the purpose of this experiment the specimens were 100mm wide and therefore each shoe
 100 print was 130mm long and 100mm wide. The pressure load applied on each shoe was 0.707 MPa,
 101 which is slightly higher than the recommended by the standards. This load pressure corresponds with
 102 9.2 kN on each shoe ($0.707\text{MPa} \times 130\text{mm} \times 100\text{mm}$), which means a total of 18.4kN. If the same
 103 pressure load of 0.707MPa is applied on a wheel print type B (double tyre 220mm by 320mm), it
 104 corresponds with 100kN wheel load which is typical truck load utilized in the Netherland. [8].

105 Tests were performed under two temperatures Ranges (-5°C and $+10^{\circ}\text{C}$). The sinusoidal
 106 compression loading P ranking between F_{\max} and $0.1 \times F_{\max}$ at a frequency 4 Hz running for two
 107 million cycles.

108 The climate chamber and the specimen temperature were measured by two temperature
 109 sensors. One in the chamber to measure the chamber room temperature and one on the upper face of
 110 the porous asphalt to measure the specimen temperature.
 111



112
 113
 114 **FIGURE 6 The 5 point bending set up,**
 115

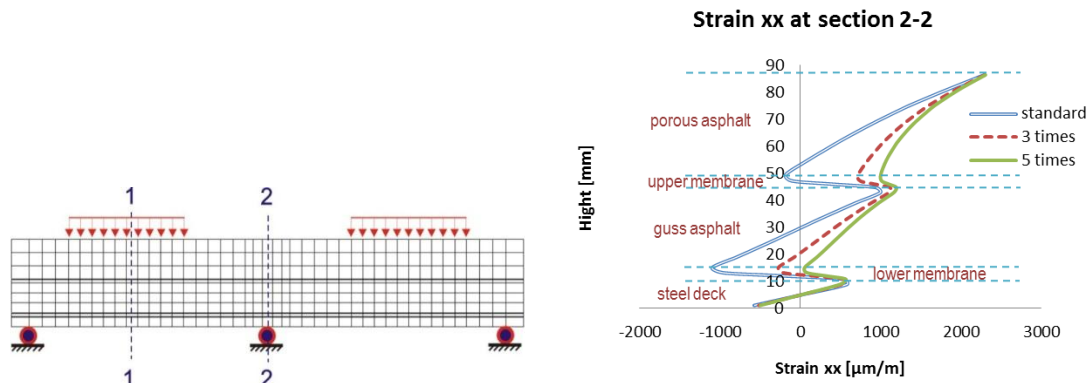
116 PRELIMINARY FINITE ELEMENT STUDY

117 In order to understand the experimental observation, preliminary finite element simulation of 5PBT
 118 was investigated first. Based on static ramp loading tests and preliminary finite element analysis using
 119 the Zener Viscoelastic model the strain distribution on the specimen are shown in Figure 7 Steel is
 120 regarded as a linear elastic material with Young's modulus 210000 MPa and the Poisson's ratio 0.2.
 121 Asphaltic surfacings and membranes are assumed to be viscoelastic material.. The model parameters
 122 for the FE simulations are listed in Table 4.

123 **Table 4 viscoelastic parameters of the materials used**

Materials used	temperature(°C)	E_1 (MPa)	E_∞ (MPa)	Poisson's ratio	η (MPa.s)
Porous asphalt	10	200	1	0.3	15750
Guss asphalt		450	3	0.3	15750
Upper/bottom membrane		9.18	5.9	0.3	267
Porous asphalt	5	2000	10	0.3	22500
Guss asphalt		4500	30	0.3	22500
Upper/bottom membrane		46	30	0.3	384

124
 125 It can be observed that the stiffness of the two membrane layers plays quite important role in
 126 combining different surfacing material layers together as a whole. Assume that the stiffness of
 127 membranes is comparable with PA or GA layers, and those layers are properly bonded together, the
 128 multilayer surfacing structure could be regarded as a composite beam. By increasing the stiffness of
 129 the membrane the strain distribution change as well as it can be seen at section 2-2 in Figure 7. The
 130 effect of stiffness is less noticeable on top of PA, however at the interface between PA and GA and
 131 between GA and steel, the effect on the tensile stress is quite recognizable.
 132

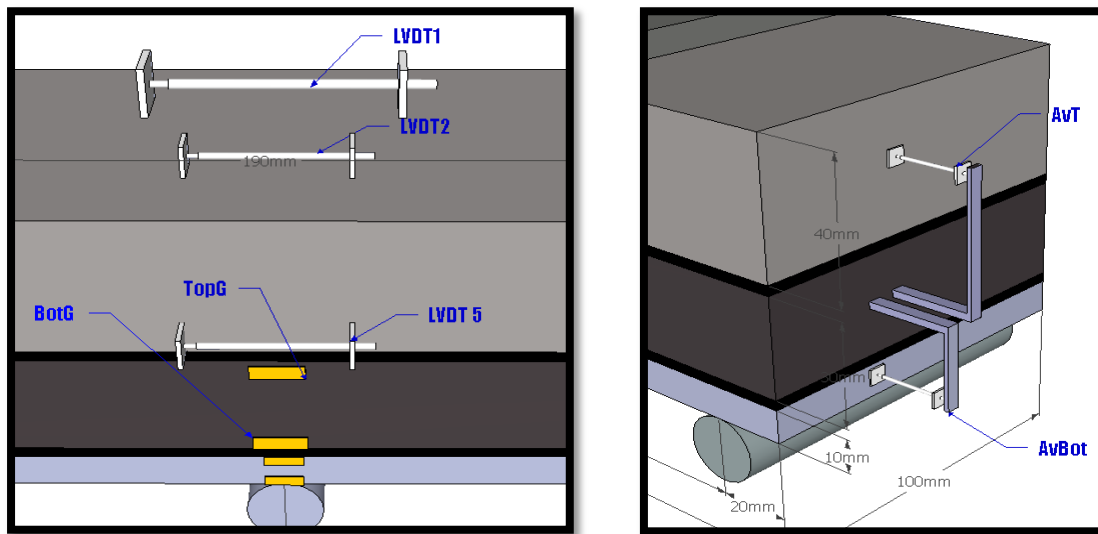


133
134

FIGURE 7 Profile of the strain distribution for all materials

135 **DISCUSSION AND RESULTS**

136 The results from two types of specimens denoted product A and B, the maximum strains and the
 137 displacements at two temperatures(-5⁰C and 10⁰C) are presented. The main concern is at the middle
 138 support where higher stress concentration occur and at the side of the specimen in order to monitor
 139 shear deformations on the asphaltic layers. Strains were monitored at two location on the front side of
 140 GA. The first one close to the top membrane referred as (TopG) and the second close to the bottom
 141 membrane referred (BotG). Strain measurements on steel plate are also monitored. Displacements
 142 were measured on the top face of PA via LVDT sensors (LVDT1 and LVDT2). Shear displacement
 143 measurements between PA and GA is denoted as (AvT). The shear displacement measurement
 144 between GA and steel is denotes as (AvBot). The schematic of specimen instrumentation is shown in
 145 Figure 8



146

147 **FIGURE 8** Location of Strain gauges and LVDTs

148 *Strain measurements*

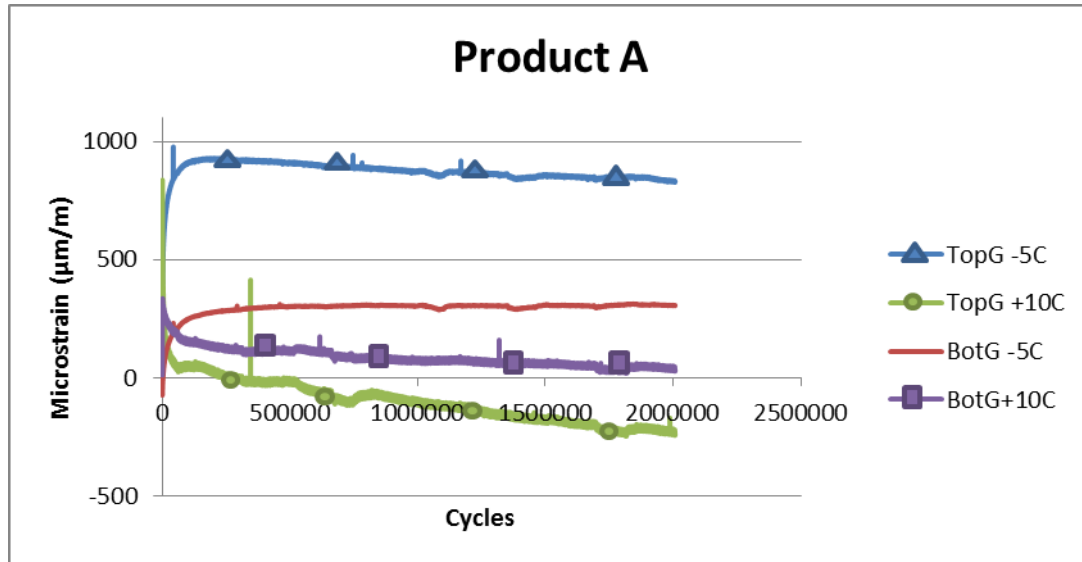
149 In Figures 9 and 10 the results from the strain measurements over cycle counts for product A and B
 150 are presented. Strains are measured on the top and bottom side of the GA as it can be seen in Figure 9
 151 for two temperatures, -5⁰C and 10⁰C.

152

153

154

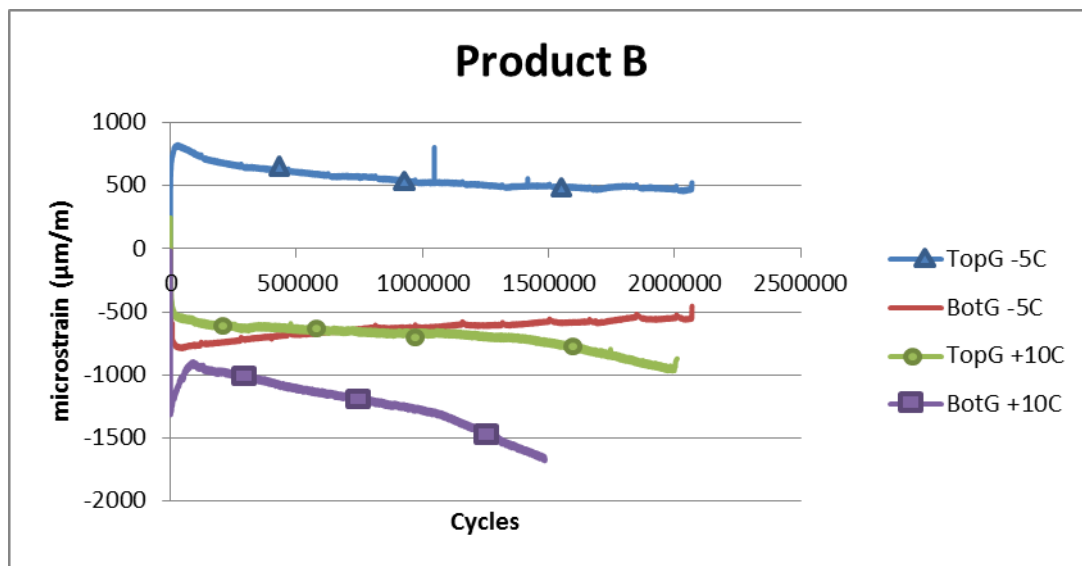
155 From Figure 9 it can be observed that higher tensile strength occur at the top of GA at -
 156 5°C .During the first 50.000 cycles the strain gradually increased so to reach a maximum value
 157 around 900µm/m and then a slight decrease until the end of the test. The same observation can be
 158 made for the (BotG) measurement though the maximum strain is around 300µm/m and after the first
 159 50,00 cycles the strain stabilized there. For both temperatures higher levels of strain concentration
 160 occur at the top face of the Guss asphalt (TopG).



161

162 **FIGURE 9 micro-strain measurements on Guss asphalt for product A**

163 For product B in Figure 10, the strain concentration at the TopG location found to be higher
 164 as well for -5°C, around 800µm/m. For the BotG location at -5°C the magnitude of strain
 165 concentration is more or less the same as on the TopG location at +10°C and the presence of the
 166 compression strain for both temperatures can be explained by using finite element analysis of
 167 composite beam in Figure 7. Strain measurements on BotG at 10°C after 1.8 million cycles have not
 168 been recorded because of the existence of cracks. As it can be seen though from the trend of the line,
 169 immediately after loading the strain magnitude decrease to 800µm/m and then exponential decrease.



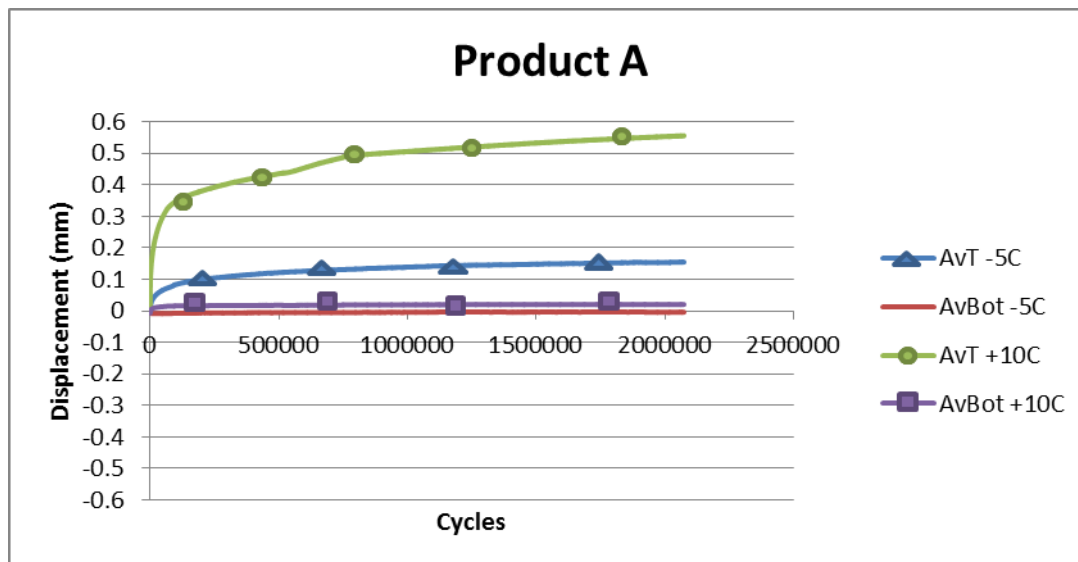
170

171 **FIGURE 10 micro-strain measurements on Guss asphalt for product B**

172

173 *Displacement measurements*

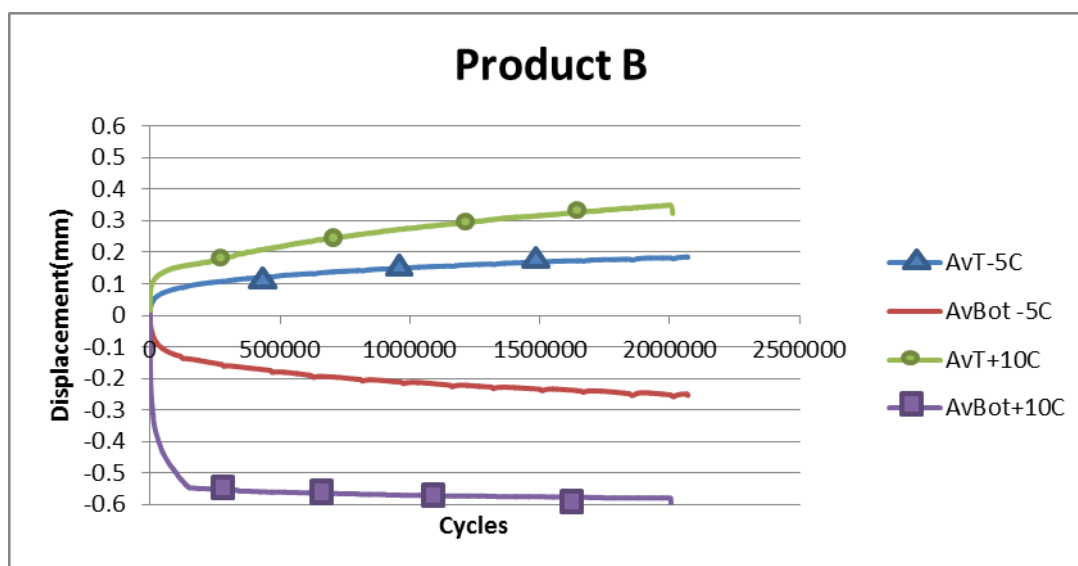
174 Four sets of LVDTs have been installed at both sides of the samples to measure the shear
 175 displacement between the asphalt layers but also the relative displacement between the GA and the
 176 steel deck. An average value from both side measurements for both interfaces has been used for the
 177 graphical representation.



178

179 **Figure 11 Shear displacement on PA/GA and GA/steel interface, product A**

180 Figure 11 shows that the relative deformation between the (GA) and the steel is quite small for
 181 specimen with product A, especially at -5°C is almost zero resulting no significant change during the
 182 entire fatigue test. However the temperature seems to have great influence on the GA/PA interface,
 183 especially at the temperature of 10°C for the average top shear displacement. The influence of the top
 184 membrane on the structure is significant compared the shear displacement values at both temperature.

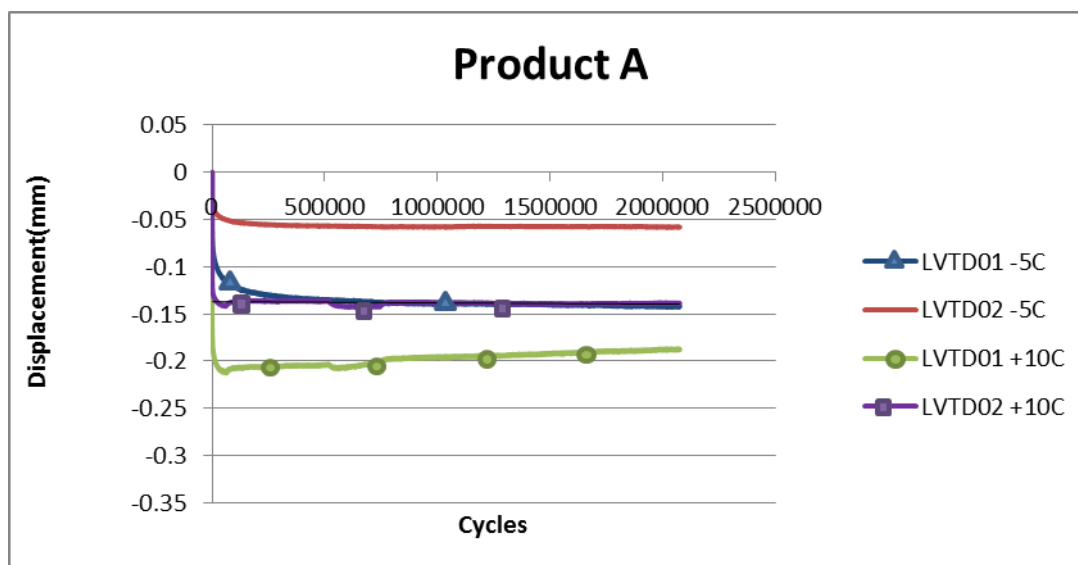


185

186 **FIGURE 12 Shear displacement on PA/GA and GA/steel interface, product B**

187 The shear displacements for product B are presented in Figure 12. In this case significant
 188 influence of the temperature is observed both for the PA/GA and GA/steel interface. By comparing
 189 the average bottom shear displacements between GA and steel and the average top shear displacement
 190 between PA and GA it can be observed that the bottom membrane gets higher influence from the

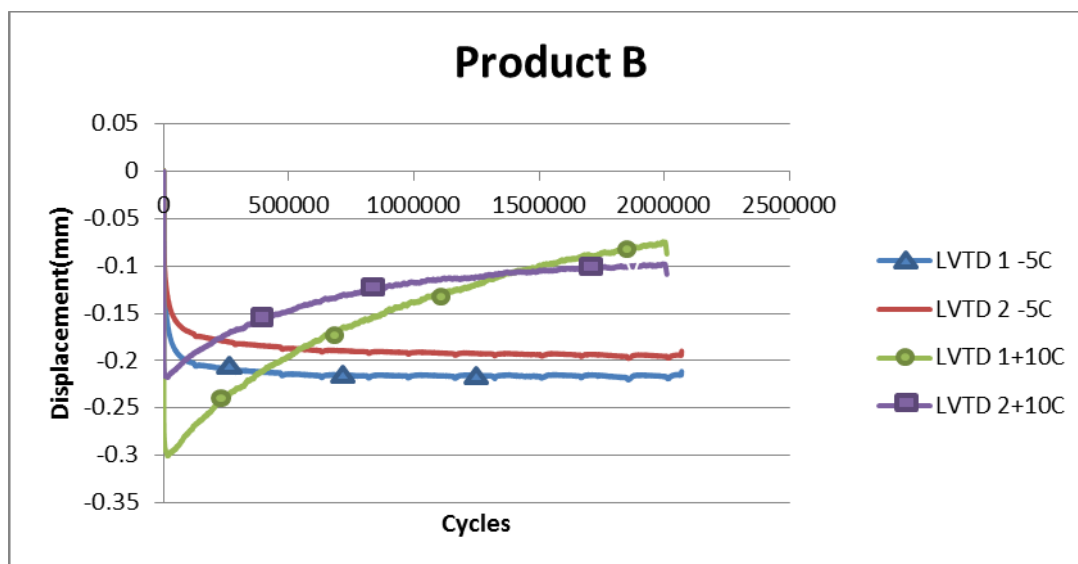
191 difference of temperature and it results the higher shear displacement increment. The top shear
 192 displacement is higher at 10⁰C as it was expected.



193

194 **FIGURE 13 Displacement measurements on Porous asphalt, product A**

195 In Figures 13 and 14 the results from the LVDT measurements over cycle counts for product A
 196 and B are presented. As it was explained earlier both LVDT1 and LVDT2 are placed at the top face of
 197 the specimen over the central support. LVDT 1 is exact at the middle of the specimen though LVDT 2
 198 is placed half way from the LVDT1 and the front edge. From Figure 13 we can observe that Both
 199 LVDTs measurements show the appearance of compression deformation at the central location and
 200 this can be explained taking into account the nature of the porous asphalt material and the actual
 201 position of the LVDTs. Both of them are placed at the top face close to the loading area where the
 202 viscous deformation of the porous asphalt material may squeeze the porous asphalt material between
 203 the two loading platen hence produce compression deformation at the central location



204

205 **FIGURE 14 Displacement measurements on Porous asphalt, product B**

206 From the LVDTs measurements in Figure 14 for specimen with product B, similar
 207 observations as specimen with product A in Figure 13 can be observed. The compression deformation
 208 instead of tension deformation are present on the top side of the PA at the location between the

209 loading area. At temperatures below zero both LVDT measurements show an exponentially increase
210 during the first 70,000 cycles which finally stabilized during the test. At 10⁰C both LVDTs monitor
211 higher levels of displacements during the first 80,000 cycles which is followed by a gradual decrease
212 until the end of the test. This decrease shows that elastic recovery occur at the mix after certain
213 loading time.

214 CONCLUSIONS

215 The main findings that can be drawn from the results presented in this paper are summarized as
216 follows.

- 217 • The five-point bending test offers a good tool in studying the composite behavior of the
218 multilayer surfacing system on orthotropic steel deck bridges;
- 219 • The elastic model cannot be fully applicable in order to simulate accurately the response of
220 the surface material. The Zener viscoelastic model is essential.
- 221 • Detection of top to bottom cracks for product B at 10⁰C.
- 222 • Specimen with product B was found to have higher compressive strain concentration values
223 at 10⁰C.
- 224 • Due to the viscous effect of asphalt surfacings, the compression deformation instead of
225 tension deformation occurs on the top side of the PA at the central location between the
226 loading area. The criteria of judgment of specimen failure at the location where it is subjected
227 to negative moments is not applicable.

228 ACKNOWLEDGMENT

229 This work is part of the research program of InfraQuest. InfraQuest is a collaboration between
230 Rijkswaterstaat, TNO and the Delft University of Technology. This research project is partially funded
231 by the Dutch Transport Research Centre (DVS) of the Ministry of Transport, Public Works and Water
232 Management (RWS). Their financial support is highly appreciated.

233 REFERENCE

- 234 1. Gurney, T., *Fatigue of steel bridge decks*, 1992, HMSO Publication Centre: London. p. 165.
- 235 2. Mangus, A.R. and S. Sun, *Orthotropic Bridge Decks*. Bridge Engineering Handbook, ed. W.
236 Chen and L. Duan 1999, Boca Raton: C.R.C. Press.
- 237 3. Houel, A. and L. Arnaud, *A five point bedding test for asphalt cracking on steel plates*, 2008,
238 Taylor & Francis Group, London . p. 261-270..
- 239 4. Hameau, G., C. Puch, and A.M. Ajour, *REVETEMENTS DE CHAUSSEES SUR*
240 *PLATELAGES METALLIQUES - 2 - COMPORTEMENT A LA FATIGUE EN FLEXION*
241 *SOUS MOMENT NEGATI* 1981.
- 242 5. Medani, T.O., *Design principles of surfacings on orthotropic steel bridge decks*, 2006, Delft
243 University of Technology: Delft.
- 244 6. Pouget, S., et al., *Numerical simulation of the five-point bending test designed to study*
245 *bituminous wearing courses on orthotropic steel bridge*. *Materials and Structures*, 2010. 43(3):
246 p. 319-330.
- 247 7. Houel, A., T.L. N'Guyen, and L. Arnaud, *Monitoring and designing of wearing courses for*
248 *orthotropic steel decks throughout the five-point bending test*. *Advanced Testing and*
249 *Characterisation of Bituminous Materials*, Vols 1 and 2, 2009: p. 433-442.
- 250 8. Freitas, T.d., *Steel plate reinforcement of orthotropic bridge decks*, in *Structural and Building*
251 *Engineering, Civil Engineering and Geosciences* 2012, Delft University of Technology: Delft.
- 252 9. Liu, X., Medani, T.O., Scarpas, A., Huurman, M. and Molenaar, A.A.A. "Experimental and
253 numerical characterization of a membrane material for orthotropic steel deck bridges: Part 2
254 - Development and implementation of a nonlinear constitutive model," *Finite Elements in*
255 *Analysis and Design*, vol. 44, pp. 580-594, June 2008.

- 256 10. Liu,X., Scarpas,A. "Experimental and numerical characterization of a membrane adhesive
257 bonding strength on orthotropic steel deck bridges:Part 1, ,2012: pp. 11-23
258
259